International Journal of Heat and Fluid Flow 29 (2008) 1054–1059

Contents lists available at ScienceDirect

International Journal of Heat and Fluid Flow

journal homepage: www.elsevier.com/locate/ijhff

Onset of vortex shedding in planar shear flow past a square cylinder

A. Lankadasu, S. Vengadesan *

Department of Applied Mechanics, IIT Madras, Chennai, Tamil Nadu 600 036, India

ARTICLE INFO

Article history:
Received 15 June 2007
Received in revised form 22 February 2008
Accepted 23 February 2008
Available online 14 April 2008

Keywords:
Square cylinder
Onset of vortex shedding
Shear parameter

ABSTRACT

Incompressible linear shear flow across a square cylinder is numerically analyzed by solving unsteady 2-D Navier–Stokes equations. Simulations are carried out for three sets of shear parameters, 0.0, 0.1 and 0.2 and two sets of solid blockage ratios, 6.25% and 10%. The aim of the present simulations is to find out the influence of shear on the onset of periodic time dependent flow, which is observed using time varying lift coefficient. With increasing shear, the critical Reynolds number, at which flow becomes time dependent, is reduced. The mean drag coefficient decreases either with increasing shear for a particular Reynolds number or with increasing Reynolds number for a particular shear parameter.

1. Introduction

The behavior of a fluid flow past a body is characterized by the relative significance of the viscous effect compared to the inertia effect. The ratio of these two effects is called Reynolds number, *Re*. The behavior of such flows, when *Re* is increased, undergoes a sequence of well established bifurcations. For example in the case of square cylinder in uniform cross flow, at very low *Re*, the flow is laminar, steady and does not separate from the cylinder. With the increasing *Re*, the flow separates from the trailing edge but remain steady and laminar up to *Re* of about 50 (Sohankar et al., 1998). Beyond this *Re*, the flow undergoes Hopf bifurcation to develop into a time dependent periodically oscillating wake. With a further increase in *Re*, localized regions of high vorticity are shed alternatively from either side of the cylinder and are convected downstream, the flow is still laminar and 2-D. Increasing the *Re* value, the flow undergoes a further bifurcation at around *Re* = 150–200 and becomes three-dimensional but remains time periodic (Robichaux et al., 1999; Sohankar et al., 1999; Saha et al., 2003; Luo et al., 2007). By increasing the Reynolds number further, the flow becomes chaotic and eventually transition to turbulence occurs. A similar sequence of bifurcations also occurs for other cross-sections like circular, elliptic, etc. (Jackson, 1987; Williamson, 1996; Balachandar and Parker, 2002; Zhang and Balachandar, 2006). The sequence of bifurcations for the case of flow over a square cylinder, when the approach flow is planar shear, is likely to be similar.

There are typical situations, when the approach flow is not uniform. For example, when a small cylinder is placed in the separated shear layer of a large main cylinder to alter the vortex shedding phenomena behind the main cylinder, the small cylinder is inevitably subjected to the effect of shear induced from the large cylinder. Onset of periodic flow from the small cylinder induces oscillatory forces on the body, which may trigger flow-induced vibration, and in turn alter the vortex shedding on the main cylinder. For the investigation of velocity gradient effects, the simplest case of a non-uniform flow is the uniform shear flow, which has a linear distribution of the longitudinal velocity component along the transverse direction. It has been shown by past investigations on circular cylinders, e.g., Jordan and Fromm (1972), Kiya et al. (1980), Kwon et al. (1992), Mukhopadhyay et al. (1999), Xu and Dalton (2001), Sumner and Akosile (2003), that the flow approaching with linear shear has greatly altered the vortex dynamics in the wake when compared to the uniform flow case. They attributed this to the constant vorticity embedded in the free-stream. For square-sectional cylindrical bodies, shear effects have been reported by, e.g., Ayukawa et al. (1993), Hwang and Sue (1997), Saha et al. (2001), Cheng et al. (2005, 2007). Ayukawa et al. (1993) conducted experiments and performed discrete vortex simulations at *Re* = 4000. They observed that with high shear parameters the flow becomes self similar downstream of the cylinder. Saha et al. (2001) studied numerically the same problem for wide range of Reynolds numbers. They showed that due to influence of shear, Karman vortex street mainly consists of clockwise vortices, whose decay is very slow when compared to that of uniform flow. However, in their study the lateral width, *w*, of the flow domain was restricted such that the streamwise velocity in the free-stream was

* Corresponding author. Tel.: +91 44 22574063; fax: +91 44 22574052.
E-mail address: vengades@iitm.ac.in (S. Vengadesan).

0142-727X/$ - see front matter © 2008 Elsevier Inc. All rights reserved.
doi:10.1016/j.ijheatfluidflow.2008.02.016

constantly positive ($u > 0$), that is the free-stream could not flow in the reverse direction due to the imposed shear rate. Hence, perhaps their studies are limited to low shear parameters and with high blockage ratio. Recently, Cheng et al. (2005, 2007) have reported that vortex shedding disappeared for large shear parameters. The Strouhal number decreases as the shear parameter increases. The drag coefficient tends to decrease with increasing shear parameter.

The objective of the present study is twofold. First, to investigate the onset of periodic time dependent flow the approach flow is linear planar shear across the square cylinder. To this end, the instantaneous lift coefficient is examined. Second, the blockage ratio ($B = d/w$, where d is the width of the cylinder and w is the lateral width of the computational domain) effect on the instantaneous and mean quantities are examined for two sets of blockage ratios. The non-dimensional shear parameter is defined as $K = Gd/U$, where G is the streamwise velocity gradient in the transverse direction and U is centerline velocity at the inlet. In this study, K is varied as 0.0, 0.1 and 0.2.

2. Physical and mathematical formulation

The problem under consideration in the present study is 2-D, unsteady, viscous and incompressible flow with constant fluid properties around an isolated square cylinder. The equations for continuity and momentum, in non-dimensional form, are expressed as

$$\frac{\partial u_i}{\partial x_i} = 0 \tag{1}$$

$$\frac{\partial u_i}{\partial t} + u_j \frac{\partial u_i}{\partial x_j} = -\frac{\partial p}{\partial x_i} + \frac{1}{Re} \frac{\partial^2 u_i}{\partial x_j \partial x_j} \tag{2}$$

where indices $i, j = 1, 2$ refer to the streamwise (x), and crosswise (y) directions of the Cartesian coordinate system, respectively. All geometrical lengths are normalized with size of cylinder side d, velocities with the speed of the undisturbed stream at the center of the cylinder U, physical times with d/U, and pressure with ρU^2,where ρ is the fluid density. Coefficient of drag and Strouhal number are defined as $\bar{C}_D = 2\bar{F}_D/\rho U^2$, $St = fd/U$, respectively, where $\bar{F}_D$ is the mean drag force per unit area and f is the shedding frequency.

Fig. 1 shows the computational domain. The flow is described in a Cartesian coordinating system (x and y) in which the x-axis is aligned with the inlet flow direction (streamwise direction), the y-axis is normal to the x-axis (cross-stream direction). The origin is centered at the mid point of the upstream face of the cylinder. The first grid point from the body is maintained at $0.008d$. For getting better predictions, the number of points on each face of the cylinder is fixed at 50. To adjust these points on the entire face, we followed the non-uniform distribution of nodes on the each face of the cylinder. At the corners, we maintained minimum distance and then uniformly stretched up to the center of the face from both the corners. The grid distribution in the rest of domain both in the streamwise as well as in the lateral direction was made non-uniform with constant stretching ratio. The stretching ratio is defined as ratio of large to small cell width of two consecutive cells in the respective direction. The value of the stretching ratio in all the directions is not same, but constant in the respective direction. Typical stretching ratios used in the present simulation are 30, 25 and 25 in the upstream direction, downstream direction and cross-stream direction, respectively.

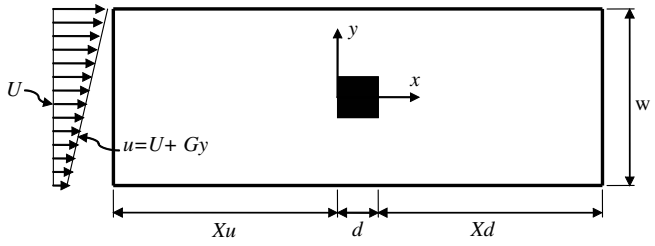

Fig. 1. Computational domain and coordinate system.

3. Numerical details

An incompressible finite difference code with staggered grid arrangement is used. After discretization, Eqs. (1) and (2) were solved with an explicit scheme. Third order upwind biased scheme for convective terms, central differencing scheme for diffusion terms and second order accurate Adams–Bashforth scheme for time marching was used. Time marching was done in two stages. In the first stage, two velocity components are calculated using previous values of velocities and pressure for all the cells. However these values do not necessarily satisfy the mass conservation criteria imposed by the continuity equation (i.e., divergence-free condition for incompressible flow). Thus, in the second stage, adjustment must be made to ensure mass conservation. This is achieved by using highly simplified marker and cell (HSMAC) algorithm (Hirt and Cook, 1972). Basic validation of the code can be found in Nakayama and Vengadesan (2002) and Kumaran and Vengadesan (2007).

The time marching calculations were started with the fluid at rest. The conditions necessary to prevent the numerical oscillations are determined from the CFL condition and the restriction on the grid Fourier number (Hwang and Sue, 1997; Saha et al., 2001). In the present study, residual of continuity equation for mass conservation, on each cell was set a maximum value of 0.0005.

At the inlet, a linear velocity profile ($u = U + Gy$, $v = 0$) is assumed, where U is the center line velocity. At outlet boundary, the convective boundary condition ($\partial u_i/\partial t + U_c(\partial u_i/\partial x_j) = 0$) is used for both velocity components, where U_c is the convective speed and in the present work it is space-averaged streamwise exit velocity. No-slip conditions are prescribed at the body surface. At top and bottom boundaries, in the present work, we have used $\partial u/\partial y = K, v = 0$ (Kang, 2006; Lankadasu and Vengadesan, 2007). It should be noted that, if the K value is zero, this condition results in symmetry condition which is the most commonly used far field boundary condition (for example, Saha et al., 1999).

4. Validation

In order to validate the present code, first we performed simulation of uniform flow past a square cylinder at Reynolds number 100 and compared with the available results. Sufficient literature is available for the same test case. Compilation of domain size and flow parameters used in these previous studies is presented in Table 1. Except Cheng et al. (2005, 2007), all the remaining authors considered here, had restricted their lateral width, to avoid the negative velocity condition on the lower side at the far field boundary for high inlet shear rate. Similarly, in the present study the lateral width is also restricted to some finite value to keep the inlet velocity always positive. Extent of the domain size on the upstream side of the cylinder is varied from 5 to 40 times of the cylinder width (or diameter). For the validation purpose, the inlet domain is fixed at $10d$.

It is well known fact that, selection of outlet boundary condition dictates the downstream domain size. The main aim of the downstream distance and exit boundary condition is that, it should not disturb the outgoing flow. It has been shown that Neumann boundary condition (gradient free) requires considerably longer

Table 1
Compilation of computational parameters: *Re*, Reynolds number based on the centerline velocity; *w*, lateral width; *Xu*, distance for leading edge to inlet; *X*, total length of the domain in the streamwise direction; *K*, shear parameter; NU, non-uniform grid; SC, square cylinder; CC, circular cylinder

References	*Re*	*K*	*w*	*Xu*	*X*	δ	Grid	Body
Hwang and Sue (1997)	500–1500	0–0.25	8	5	20	0.01	NU	SC
Saha et al. (1999)	250–1500	0–0.2	10	–	40	–	U	SC
Cheng et al. (2005)	100	0–0.5	25	12	43	–	NU	SC
Kang (2006)	50–160	0–0.2	10	40	80	0.017	NU	CC
Kwon et al. (1992)	600–1600	0–0.25	15–6.2	–	–	–	–	CC
Kiya et al. (1980)	35–1500	0–0.25	37–6	–	–	–	–	CC
Lei et al. (2000)	80–1000	0–0.25	8	5	30	0.017	NU	CC
Present	35–47	0–0.2	10&16	20	40	0.008	NU	SC

distance compared to the convective boundary condition. In the present study, convective boundary condition has been used, hence, 20*d* downstream of the body is sufficient for this low *Re* number study (Sohankar et al., 1998).

The lateral width, *w* of the domain considered in this study is 10 and 16 times of cylinder width, *d*. For these lateral widths, the solid blockage ratio calculated using $B = d/w$ is 10% and 6.25%, respectively. The criterion for selection of the blockage ratio is that, velocity should always be positive at the inlet for all the shear parameters considered in this study. Hence, $K = 0.2$ case is studied with $B = 10\%$ only, as $B = 6.25\%$ results in negative velocity.

Influence of the first grid point (δ) on the results is also studied. We consider two values viz. $\delta = 0.007d$ and $0.008d$. For both the grids, we used same stretching factor and also maintained same ratio of the largest width of the cell to the smallest width of the cell in the domain. With these constraints, we arrived 226×195 for $\delta = 0.008$ and 260×220 for $\delta = 0.007d$. These δ values are less than or equal to the δ used in the literature (see, Table 1). A constant non-dimensional time step, $\Delta t = 0.0005$ used in the present simulation has largely satisfied the requirement to capture all the frequencies involved in this flow. Results obtained using these two grids are given in Table 2. For both the grids, the global parameters like $\bar{C}_D$ and *St* are same up to second and third digit, respectively. Whereas, sensitive parameter like root mean square value of the lift coefficient is varied approximately 1.25%. Hence, for further calculation, we considered the grid of 226×195. Calculated global parameters like mean drag coefficient, Root mean square value of the lift coefficient and Strouhal number using the present grid and the computational domain (see, Fig. 1) with the blockage ratio, $B = 6.25\%$ are compared with the available literature for $Re = 100$ and $K = 0.0$ in the Table 3. The small discrepancy among the results is attributed to the different solid blockage ratios, boundary conditions, domain size, grid resolution and numerical schemes. Except Okajima (1982), all other authors used numerical simulations. Our simulated results match reasonably well with the recently published results. Further validation of the code with inlet shear flow past the bluff body is reported in Lankadasu and Vengadesan (2007).

Table 2
Comparison of calculated global parameters with available literature for $Re = 100$ and $K = 0.0$

References	*St*	$C_{L,rms}$	$\bar{C}_D$	Δt
Okajima (1982)	0.135–0.140	–	–	
Davis and Moore (1982)	0.154	–	1.64	0.05
Franke and Schonung (1990)	0.154	–	1.61	0.025
Kelkar and Patankar (1992)	0.13	–	1.80	0.125
Sohankar et al. (1998)	0.146	0.156	1.47	0.025
Robichaux et al. (1999)	0.154	–	1.53	
Jan and Sheu (2004)	0.144	–	–	0.01
Cheng et al. (2007)	0.144	0.152	1.44	
Present	0.143	0.159	1.47	0.0005

Except Okajima (1982) all are numerical results.

Table 3
Grid independence study at $Re = 100$, $K = 0.0$, $\Delta t = 0.0005$ and $B = 6.25\%$: δ is the first grid point from the cylinder

$I \times J$	δ	$\bar{C}_D$	$C_{L,rms}$	*St*
226×195	0.008	1.47	0.159	0.143
260×220	0.007	1.47	0.157	0.143

Table 4
Comparison of mean quantities between two inlet domain sizes with blockage ratio 10%

Shear parameter	*Re*	$B = 10\%$					
		$Xu = 10d$			$Xu = 20d$		
		St	$\bar{C}_D$	$\bar{C}_L$	*St*	$\bar{C}_D$	$\bar{C}_L$
$K = 0.0$	45	–	–	–	–	1.602	0.000
	47	–	–	–	0.122	1.579	0.000
	44	–	1.604	0.000	–	–	–
	46	0.130	1.588	0.000	–	–	–
$K = 0.1$	42	–	–	–	–	1.577	−0.077
	44	–	–	–	0.122	1.555	−0.071
	40	–	1.608	−0.084	–	–	–
	42	0.122	1.592	−0.081	–	–	–
$K = 0.2$	38	–	–	–	–	1.527	−0.147
	40	–	–	–	0.107	1.514	−0.140
	35	–	1.579	−0.164	–	–	–
	37	0.114	1.560	−0.157	–	–	–

Since the present simulations with inlet shear condition are carried out at much lower Reynolds number than $Re = 100$, it is essential to ascertain the sufficiency of the inlet domain size. For this purpose, we considered two inlet domain sizes viz. $Xu = 10d$ and $20d$ and results are compared in Table 4. The Reynolds number corresponds to before and after the critical Reynolds number for a particular inlet domain size. This otherwise means the inlet domain length has influence on the critical Reynolds number. Correspondingly, the mean quantities also showed dependence. The inlet domain size further increased to $25d$ and found negligible difference between $20d$ and $25d$. Hence, finally $20d$ has been selected for the rest of the calculations.

5. Results and discussion

For a particular Reynolds number, simulation starting from the rest eventually reaches steady or unsteady state depending on the Reynolds number value. For identification of onset of periodic flow, we have taken instantaneous lift coefficient as the basis. Many unsteady simulations have been done to identify the onset of periodic time dependent flow phenomenon. Different simulations correspond to different Reynolds numbers, and for every case, it is increased in steps of two. Therefore, the actual critical Reynolds

number falls in between. Hence, the predicted critical Reynolds numbers, Re_{cr} have an error bar of ±1. Though the bifurcation or stability analysis also gives critical Reynolds number, it does not reveal flow developing features. Suppose if *Re* is below the critical Re_{cr}, it approaches steady state after disturbance due to the initial conditions died out, whereas, if it is above the critical *Re*, the disturbance is amplified and reaches a stable periodic time dependent flow. The transition behavior is characterized by the velocity and

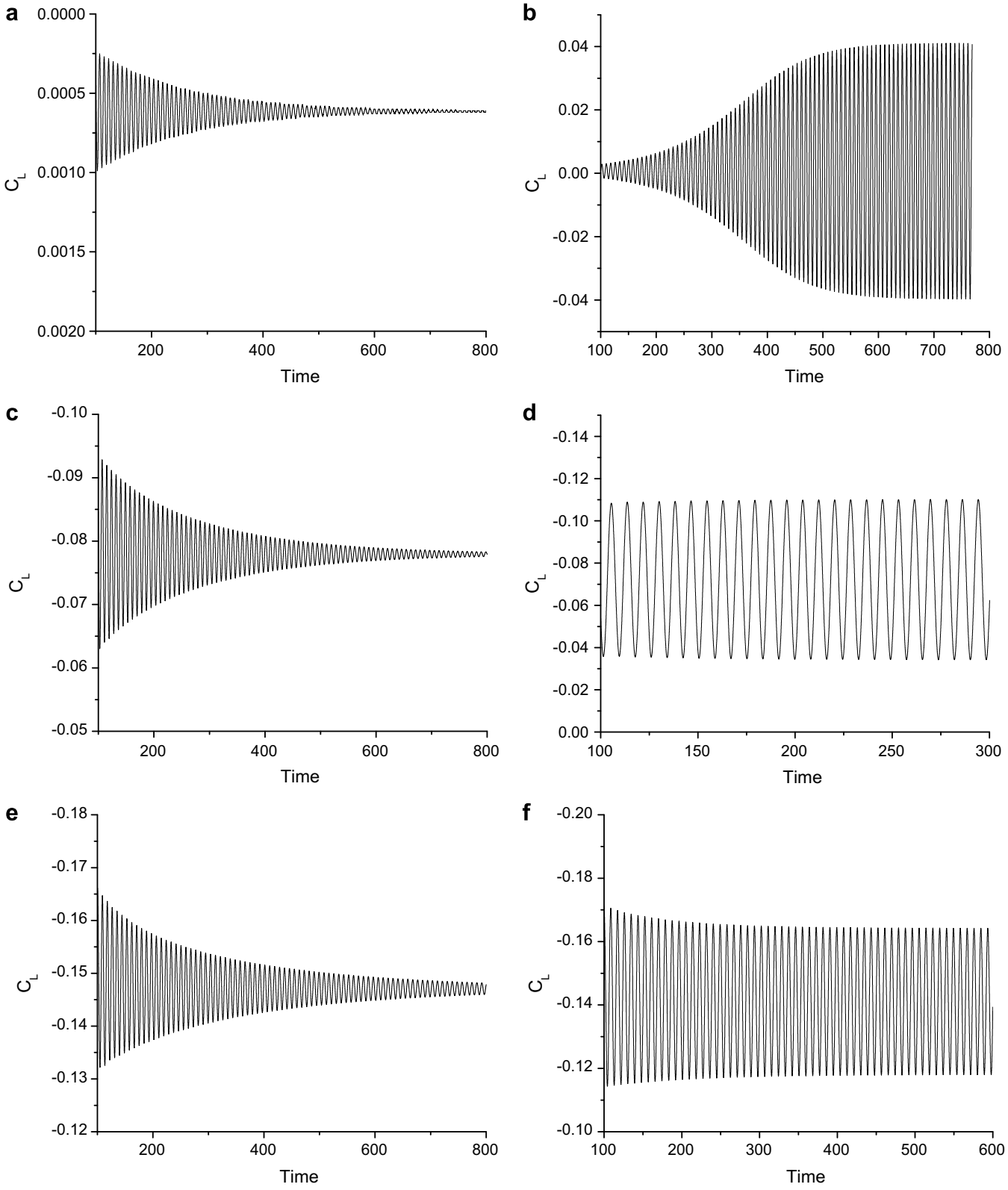

Fig. 2. Instantaneous lift coefficient before and after critical Reynolds number: (a) $K = 0.0$, $Re = 45$; (b) $K = 0.0$, $Re = 47$; (c) $K = 0.1$, $Re = 42$; (d) $K = 0.1$, $Re = 44$; (e) $K = 0.2$ $Re = 38$; (f) $K = 0.2$, $Re = 40$.

pressure signals. Results are analyzed and discussed with the help of instantaneous lift signal, instantaneous spanwise vorticity, mean drag and lift coefficients.

5.1. Variation of lift coefficient

Fig. 2 shows the variation of instantaneous lift coefficient with time for six Reynolds numbers and blockage ratio of 10% for the case of uniform flow, i.e., without shear ($K = 0.0$). Fig. 2a and b is for Reynolds number, $Re = 45$ and 47. Sohankar et al. (1998) and Kelkar and Patankar (1992) have reported that the flow is steady at this Reynolds number. Our present simulations also confirmed the same for $Re = 45$ but, unsteady behavior for $Re = 47$. The amplitude of the lift variation about the mean is continuously decreasing with time and finally approaching the zero for $Re = 45$. Even though the magnitude of lift coefficient is very small, our objective is to show that the trend is followed. In contrast to the previous one, the amplitude of the instantaneous lift coefficient from the mean is increasing with time. From the above observations, we can conclude that critical Reynolds number, at which onset of periodic vortex shedding occurs should be in between these two Reynolds numbers. Hence, we can say that critical Reynolds number is $Re_{cr} = 46 \pm 1$.

Now we carry out simulations to study the influence of shear parameter on the Re_{cr}. Fig. 2c and d is for variation of instantaneous lift coefficient for shear parameter $K = 0.1$. The simulation is initiated with uniform velocity throughout the domain except at inlet boundary where uniform shear along the lateral direction is imposed. As the simulation progresses, the flow gets adjusted to the real state. During this initial developing period, the flow experiences lot of disturbance. Due to these initial disturbances, the lift coefficient exhibited initially high magnitude of oscillations, but with evolution of flow it gets accommodated to the flow features. For the considered blockage ratio, the flow at the bottom far field of the domain is positive. Due to the shear, it is observed that mean coefficient of lift becomes negative. This trend is consistent with those reported in the literature on both square as well as circular cylinder, e.g., Cheng et al., 2007; Kang, 2006. Fig. 2c and d exhibit steady and unsteady behaviors, respectively. Therefore, critical Reynolds number is in between 42 and 44, i.e., $Re_{cr} = 43 \pm 1$. When $K = 0.1$, the lift coefficient has reached periodic state much earlier than that in the case of uniform flow.

Variation of instantaneous lift coefficient for shear parameter $K = 0.2$ is shown in Fig. 2e and f. The mean lift coefficient further shifted to the negative side at $Re = 38$, the lift coefficient becomes steady, whereas at $Re = 40$ it is time periodic time dependent. Therefore, the critical Reynolds number is within $Re_{cr} = 39 \pm 1$. From the above observation, one can conclude that critical Reynolds number decreases with increasing shear parameter.

5.2. Instantaneous vorticity

Fig. 3 shows the instantaneous spanwise component of vorticity for $K = 0.0$, 0.1 and 0.2 at Reynolds number corresponding to before and after the critical Reynolds number. Fig. 3a, c and e is before the critical Reynolds number and the vorticity is steady. For a particular value of K with increasing Reynolds number, the instability developed in the far field. Eventually, the flow becomes time dependent. Fig. 3b, d, and f is after the critical Reynolds number and there is unsteadiness in the vorticity. Unsteadiness is developed in the far field and propagating towards the cylinder. When $K = 0.0$, there is no separation at the leading edge, which has also been observed from the previously reported studies carried out near by this Reynolds number (Sohankar et al., 1997). With increasing K, the approaching velocity magnitude is different on the top and bottom sides thus the wake becomes asymmetric about the center line. The wake is tilted towards the lower velocity side and the stagnation point has moved towards the higher velocity side on the front face. Because of this, there is a separation of shear layer from the bottom leading edge when $K = 0.2$ and top shear layer still remains attached to the cylinder. This might be the cause for negative mean lift coefficient with increasing shear parameter.

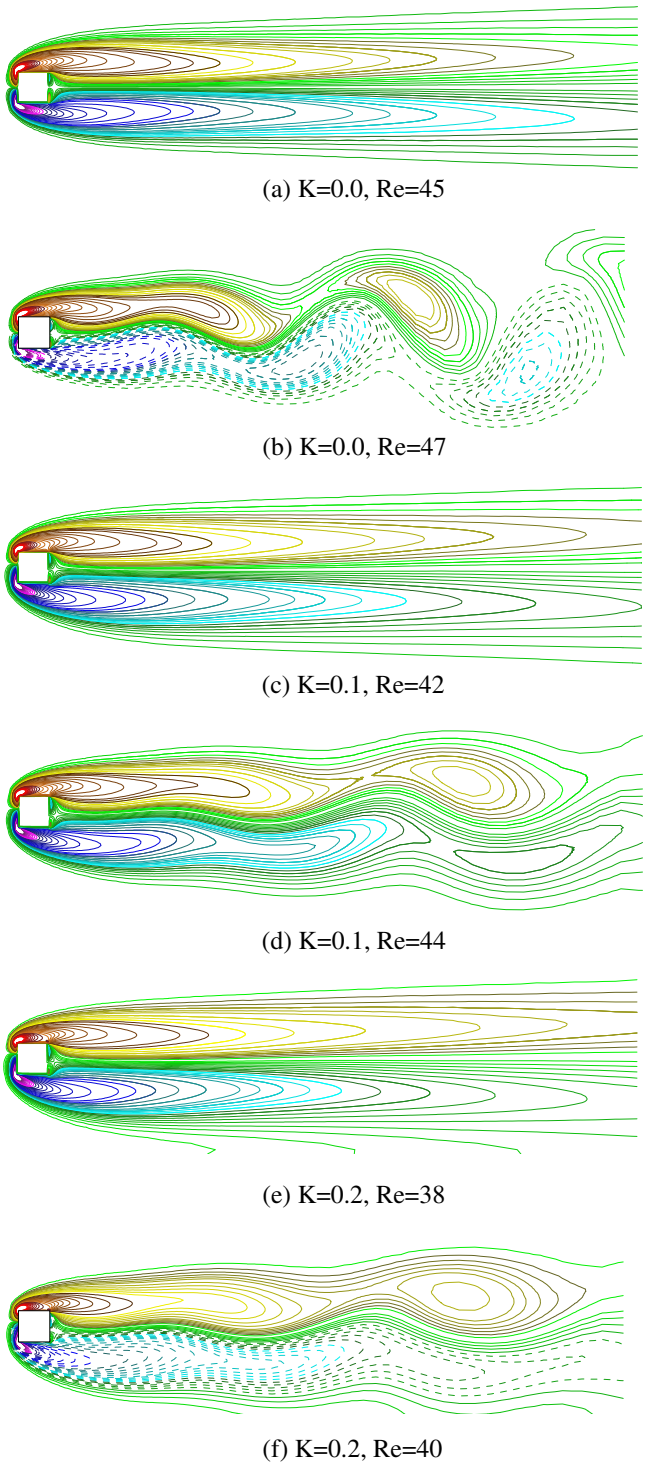

Fig. 3. The contours of instantaneous spanwise component of vorticity for $B = 10\%$: contour levels are $\omega = \pm 0.5, \pm 1, \pm 5$ and $\Delta\omega_y = 0.05$, 0.1, and 0.2, respectively.

Table 5
Comparison of mean quantities between two blockage ratios

	Re	*Xu* = 20*d*					
		B = 6.25%			*B* = 10%		
		St	$\bar{C}_D$	$\bar{C}_L$	*St*	$\bar{C}_D$	$\bar{C}_L$
K = 0.0	45	–	–	–	–	1.602	0.000
	47	–	–	–	0.122	1.579	0.000
	44	–	1.447	0.000	–	–	–
	46	0.122	1.438	0.000	–	–	–
K = 0.1	42	–	–	–	–	1.577	−0.077
	44	–	–	–	0.122	1.555	−0.071
	40	–	1.420	−0.094	–	–	–
	42	0.107	1.416	−0.091	–	–	–
K = 0.2	38	–	–	–	–	1.527	−0.147
	40	–	–	–	0.107	1.514	−0.140

5.3. Influence of blockage

In order to understand the influence of blockage ratio on the results, calculations are carried out with two blockage ratios viz. 10% and 6.25%. For both the blockage ratios, inlet domain size is fixed at *Xu* = 20*d*. At the blockage ratio of 6.25% and for *K* = 0.2, there is a negative velocity at the lower velocity side of the cylinder and hence this case is avoided. The mean quantities and critical Reynolds number are compared in Table 5. The blockage ratio has an effect on the critical Reynolds number as well as on the mean quantities. For the uniform flow (*K* = 0.0), the critical Reynolds number is observed at 46 ± 1 and 45 ± 1, respectively, when *B* = 10% and 6.25%. These critical values are lower than those reported by Sohankar et al. (1998) and Kelkar and Patankar (1992). Sohankar et al. (1998) placed the critical Reynolds number at 51.2 ± 1 with 5% blockage ratio using linearized Stuart–Landau equation. Kelkar and Patankar (1992) reported critical *Re* = 53 with 14.2% blockage ratio. Norberg and coworkers (taken from Sohankar et al., 1998) have estimated the critical Reynolds number to be in the range Re_{cr} = 47 ± 2. When *K* = 0.1, the critical Reynolds numbers are observed at 43 ± 1 and 41 ± 1, respectively for *B* = 10% and 6.25%. Strouhal number is unaffected when *K* = 0.0, but it reduced to *St* = 0.107 from 0.122 when *K* = 0.1 and *B* = 6.25%. The mean drag coefficient is increasing with increasing blockage ratio. For both the blockage ratios, the mean lift coefficient is negative when *K* = 0.1.

6. Conclusions

In the present study, time dependent calculations for a two dimensional flow around a square cylinder with a linear shear at the inlet have been carried out. The purpose of the simulations is to identify the critical Reynolds number at which the flow becomes periodic time dependent when the inlet flow is subjected to linear shear and the corresponding effect on the mean drag coefficient. For uniform approach flow (*K* = 0.0), calculated critical Reynolds number reasonably agrees with the literature. With increasing shear parameter, the critical Reynolds number and mean drag coefficient decreases. Two blockage ratios are considered to identify the possible dependency of the critical Reynolds number. Both critical Reynolds number and mean drag coefficient are found to increase with increasing blockage ratio. This is the first such reported study to consider the effect of inlet shear and blockage ratio on critical Reynolds number.

References

Ayukawa, K., Ochi, J., Kawahara, G., Hirao, T., 1993. Effect of shear rate on the flow around a square cylinder in a uniform shear flow. J. Wind Eng. Indust. Aero. 50, 97–106.

Balachandar, S., Parker, S.J., 2002. Onset of vortex shedding in an inline and staggered array of rectangular cylinders. Phys. Fluids 14, 3714–3732.

Cheng, M., Tan, S.H.N., Hung, K.C., 2005. Linear shear flow over a square cylinder at low Reynolds number. Phys. Fluids 17, 078103.

Cheng, M., Whyte, D.S., Lou, J., 2007. Numerical simulation of flow around a square cylinder in uniform-shear flow. J. Fluids Struct. 23, 207–226.

Davis, R.W., Moore, E.F., 1982. A numerical study of vortex shedding from rectangles. J. Fluid Mech. 116, 475–506.

Franke, R., Schonung, B., 1990. Numerical calculation of laminar vortex shedding flow past cylinders. J. Wind Eng. Indust. Aero. 35, 237–257.

Hirt, C.W., Cook, J.L., 1972. Calculating three-dimensional flow around structures and over rough terrain. J. Comp. Phys. 10, 324–340.

Hwang, R.R., Sue, Y.C., 1997. Numerical simulation of shear effect on vortex shedding behind a square cylinder. Int. J. Numer. Meth. Fluids 25, 1409–1420.

Jackson, C.P., 1987. A finite element study of the onset of vortex shedding in flow past variously shaped bodies. J. Fluid Mech. 182, 23–45.

Jan, Y.J., Sheu, T.W.H., 2004. A numerical configuration of the dual body vortex flowmeter design. Comput. Fluids 33, 1157–1174.

Jordan, S.K., Fromm, J.E., 1972. Laminar flow past a circle in a shear flow. Phys. Fluids 69, 972–979.

Kang, S., 2006. Uniform shear flow over a circular cylinder at low Reynolds numbers. J. Fluids Struct. 22, 541–555.

Kelkar, K.M., Patankar, S.V., 1992. Numerical prediction of vortex shedding behind a square cylinder. Int. J. Numer. Meth. Fluids 14, 327–341.

Kiya, M., Tamura, H., Arie, M., 1980. Vortex shedding from a circular cylinder in moderate Reynolds number shear flow. J. Fluid Mech. 101, 721–735.

Kumaran, M., Vengadesan, S., 2007. Flow characteristics behind rectangular cylinders placed near a wall. Numer. Heat Trans. – Part A 52 (7), 643–660.

Kwon, S., Sung, H.J., Hyun, J.M., 1992. Experimental investigation of uniform shear flow past a circular cylinder. J. Fluids Eng. (ASME) 114, 457–460.

Lankadasu, A., Vengadesan, S., 2007. Interference effect of two equal size square cylinders in tandem arrangement: with planar shear flow. Int. J. Numer. Meth. Fluids, doi:10.1002/ftd.1670.

Lei, C., Cheng, L., Kavanagh, K., 2000. A finite difference solution of the shear flow over a circular cylinder. Ocean Eng. 27, 271–290.

Luo, S.C., Tong, X.H., Khoo, B.C., 2007. Transition phenomena in the wake of a square cylinder. J. Fluids Struct. 23, 227–248.

Mukhopadhyay, A., Venugopal, P., Vanka, S.P., 1999. Numerical study of vortex shedding from a circular cylinder in linear shear flow. J. Fluids Eng. (ASME) 121, 460–468.

Nakayama, A., Vengadesan, S.N., 2002. On the influence of numerical schemes and sub-grid stress models on LES of turbulent flow past a square cylinder. Int. J. Numer. Meth. Fluids 38, 227–253.

Okajima, 1982. Strouhal number of rectangular cylinders. J. Fluid Mech. 123, 379–398.

Robichaux, J., Balachandar, S., Vanka, S.P., 1999. Three-dimensional Floquet instability of the wake of square cylinder. Phys. Fluids 11, 560–578.

Saha, A.K., Biswas, G., Muralidhar, K., 1999. Influence of inlet shear on structure of wake behind a square cylinder. J. Eng. Mech. 125, 359–363.

Saha, A.K., Biswas, G., Muralidhar, K., 2001. Two-dimensional study of the turbulent wake behind a square cylinder subject to uniform shear. J. Fluids Eng. 123, 595–603.

Saha, A.K., Biswas, G., Muralidhar, K., 2003. Three-dimensional study of flow past a square cylinder at low Reynolds number. Int. J. Heat Fluid Flow 24, 54–66.

Sohankar, A., Norberg, C., Davidson, L., 1997. Numerical simulation of unsteady low-Reynolds number flow around rectangular cylinders at incidence. J. Wind Eng. Indust. Aero., 189–201.

Sohankar, A., Norberg, C., Davidson, L., 1998. Low Reynolds number flow around a square cylinder at incidence: study of blockage, onset of vortex shedding and outlet boundary condition. Int. J. Numer. Meth. Fluids 26, 39–56.

Sohankar, A., Norberg, C., Davidson, L., 1999. Simulation of three-dimensional flow around a square cylinder at moderate Reynolds numbers. Phys. Fluids 11, 288–305.

Sumner, D., Akosile, O.O., 2003. On uniform planar shear flow around a circular cylinder at sub-critical Reynolds number. J. Fluids Strut. 18, 441–454.

Williamson, C.H.K., 1996. Three-dimensional wake transition. J. Fluid Mech. 328, 345–407.

Xu, Y., Dalton, C., 2001. Computation of force on a cylinder in a shear flow. J. Fluids Strut. 15, 941–954.

Zhang, L., Balachandar, S., 2006. Onset of vortex shedding on a periodic array of circular cylinders. J. Fluids Eng. 128, 1101–1105.